JACS
JOURNAL OF THE AMERICAN CHEMICAL SOCIETY
Article
Cite This: J. Am. Chem. Soc. 2019, 141, 6930−6936
pubs.acs.org/JACS

Counter Cations Affect Transport in Aqueous Hydroxide Solutions with Ion Specificity

Chad I. Drexler,[†,#] Tierney C. Miller,[§,#] Bradley A. Rogers,[†] Yuguang C. Li,[†] Clyde A. Daly, Jr.,[§] Tinglu Yang,[†] Steven A. Corcelli,[*,§] and Paul S. Cremer[*,†,‡]

[†]Department of Chemistry and [‡]Department of Biochemistry and Molecular Biology, The Pennsylvania State University, University Park, Pennsylvania 16802, United States

[§]Department of Chemistry and Biochemistry, University of Notre Dame, Notre Dame, Indiana 46556, United States

Supporting Information

ABSTRACT: The anomalously high mobility of hydroxide and hydronium ions in aqueous solutions is related to proton transfer and structural diffusion. The role of counterions in these solutions, however, is often considered to be negligible. Herein, we explore the impact of alkali metal counter cations on hydroxide solvation and mobility. Impedance measurements demonstrate that hydroxide mobility is attenuated by lithium relative to sodium and potassium. These results are explained by *ab initio* molecular dynamics simulations and experimental vibrational hydration shell spectroscopy, which reveal substantially stronger ion pairing between OH^- and Li^+ than with other cations. Hydration shell spectra and theoretical vibrational frequency calculations together imply that lithium and sodium cations have different effects on the delocalization of water protons donating a hydrogen bond to hydroxide. Specifically, lithium leads to enhanced proton delocalization compared with sodium. However, proton delocalization and the overall diffusion process are not necessarily correlated.

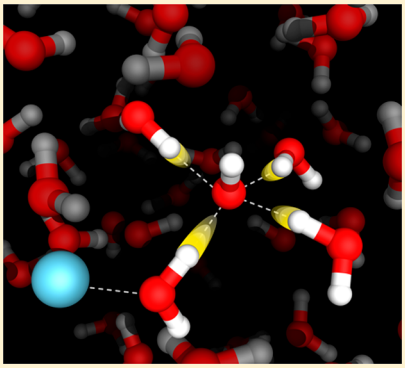

INTRODUCTION

Diffusion coefficients for ions in aqueous solutions of HCl and NaOH have been reported to be larger than those in NaCl by factors of ∼5.5 and ∼3.1, respectively.[1−4] These enhancements result from the structural diffusion of H^+ and OH^- via a Grotthuss mechanism, as opposed to the hydrodynamic diffusion of alkali metal cations and halide anions.[5−8] The difference between the acid and base enhancement factors has been widely debated. Moreover, this subject has been explored by path integral and *ab initio* molecular dynamics (AIMD) simulations capable of describing proton transfer (PT) and proton sharing between oxygen nuclei.[9,10] The general consensus is that the hydration shell structure and proton jump dynamics differ for H^+ and OH^-.[6,10−12] Conversely, vibrational spectra have long suggested similarities between acids and bases, as both display broad continuous absorption bands.[13−19]

While significant differences in hydration structure exist between aqueous H^+ and OH^-, the similarities displayed in their vibrational spectra suggest that other factors may also help to account for the disparity in the diffusion constant data. For instance, the presence and identity of counterions can impact PT. In fact, experimental and theoretical studies of HCl solutions have shown that ion pairing pulls one proton in H_3O^+ toward Cl^- at concentrations greater than 2 M.[20−23] Moreover, structural diffusion of OH^- is thought to follow a mechanism in bulk solution where the lowest energy structures contain four water molecules donating hydrogen bonds to an OH^- oxygen.[6,10] Solvent fluctuations rupture one of these four hydrogen bonds, ultimately resulting in a tetrahedral configuration around the OH^- ion that is more favorable for PT.[6,10] The role of counter cations has not been closely considered in this dynamical hypercoordination mechanism.[6,24,25]

Herein, we explore the impact of alkali metal counter cations on OH^- hydration and mobility in bulk solution. Impedance measurements show that the diffusion coefficient is attenuated by more than 20% in the presence of Li^+ compared to Na^+ and K^+ at concentrations from 10 mM to 1 M. Complementary AIMD simulations show that Li^+ cations exhibit stronger electrostatic attraction to OH^- and form more ion pairs compared to Na^+. These findings agree with Raman multivariate curve resolution (MCR) spectroscopy, which also suggests stronger ion pairing between Li^+ and OH^- compared with Na^+ or K^+. Moreover, infrared (IR) MCR spectra suggest subtly greater proton delocalization in the first hydration shell of hydroxide when Li^+ is the counterion compared to Na^+ or K^+. This is consistent with quantum mechanical calculations of the proton nuclei in the first hydration shell of hydroxide, which report enhanced proton delocalization for water molecules in solvent-shared configurations between Li^+ and OH^-. Strikingly, these findings demonstrate that ion mobility is slower in LiOH solutions compared with NaOH or KOH,

Received: December 17, 2018
Published: April 22, 2019

DOI: 10.1021/jacs.8b13458
J. Am. Chem. Soc. 2019, 141, 6930−6936

despite having more delocalized proton intensity in the corresponding IR spectrum. This is a surprising result because greater proton delocalization in the presence of Li^+ might be expected to increase solution conductivity and ion mobility. As such, cation−anion interactions would appear to be a more important factor in modulating ion mobility in this case compared to a counterion's effect on proton transfer.

RESULTS AND DISCUSSION

Counter Cations Impact Diffusion of OH^-. In a first set of experiments, we have measured the electrochemical impedance spectra (EIS) of LiOH, NaOH, and KOH solutions. The results were used to determine the corresponding diffusion coefficients as a function of salt concentration (Figure 1).

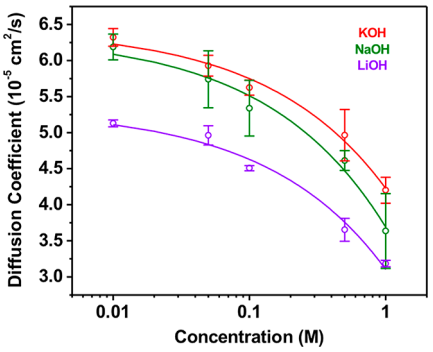

Figure 1. Effective diffusion coefficients as a function of concentration obtained by EIS. Open circles are averages, and the solid curves are fits to Onsager's model for the Kohlrausch effect (see SI). Error bars are from standard deviations of triplicate measurements.

Li^+ counter cations impede diffusion at all measured concentrations (Figure 1, purple curve), which is in agreement with previous measurements.[27] Moreover, the hydroxide salts of all three cations display a decreasing trend in ion mobility that goes as the square root of the ionic strength (see SI). While these effective diffusion coefficients incorporate hydrodynamic contributions from both the cations and hydroxide, the elevated diffusion constants compared to alkali halides are a hallmark of a structural diffusion process, i.e., a Grotthuss mechanism. The offset in mobility in the presence of Li^+ suggests that this ion may reduce the diffusion coefficient because of greater cation−hydroxide interactions. To explore this possibility further at the molecular level, we performed AIMD simulations with 1 M aqueous LiOH and NaOH solutions. At this concentration, there is greater ion pairing between Li^+ and OH^- compared to Na^+ and OH^-, as can be seen from the integrated ion number density values, $N(r)$ (Figure 2).

The cations held on average 5.88 and 3.99 hydration waters, respectively, for Na^+ and Li^+ over each 100 ps trajectory. At 1 M, there were well-defined shells of counter cations around OH^- (Figure 2, inset). The cutoff after the second shell is depicted by the dashed lines. Over this range of separation distances, cations form two distinct shells around OH^-: contact ion pairs, where the OH^- and counter cation directly interact, and solvent-shared ion pairs, where a water molecule resides in the first hydration shell of both ions.[26] Integrated number densities reveal that there are more ion pairs in LiOH solutions than in NaOH solutions over this spatial region.

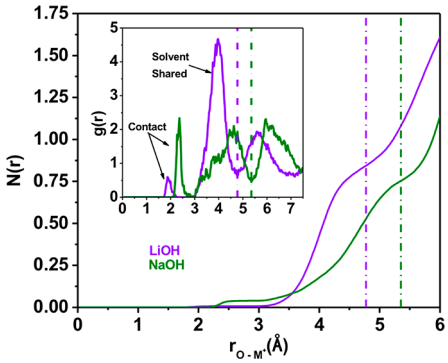

Figure 2. Integrated ion pairing number densities, $N(r)$, and the corresponding radial distribution functions (inset), $g(r)$, for 1 M LiOH (purple) and 1 M NaOH (green) calculated from AIMD simulations. The x-axis denotes the spacing between the OH^- oxygen atoms and the metal counter cation, M^+. The dashed vertical lines depict the respective second minimum for each $g(r)$.

Furthermore, the $g(r)$ plot shows that Li^+ in solvent-shared pairs resides closer to OH^- than solvent-shared Na^+ pairs. The LiOH contact ion pair peak also resides closer to OH^- than the corresponding peak for NaOH due to Li^+ having a smaller radius, although there are very few contact ion pairs. Based on these observations, it would appear that ion pairing and electrostatic attraction between Li^+ and OH^- should play a significant role in the measured diffusion differences in Figure 1. It should be noted that the $g(r)$ data and integrated ion number densities were calculated from extended 200 ps simulations, while all subsequent analyses came from the first 100 ps trajectories.

IR and Raman Spectroscopy. Structural diffusion of both OH^- and H^+ ions in water is affected by quantum mechanical delocalization of proton nuclei.[5,6,8−10] The diffusion constant data presented above might lead one to wonder whether proton sharing between the oxygen nuclei should be diminished by Li^+. As such, Raman-MCR and attenuated total reflection (ATR) IR-MCR measurements were made to better understand the impact of counter cations on OH^- and its hydration shell (Figure 3). Vibrational spectra have long been known to show very broad vibrational bands for OH^- solutions, where the low-frequency tails on the red side of the O−H stretch resonance have been attributed to shared/delocalized protons.[15]

The bulk Raman and IR spectra do not reveal an obvious counter cation dependence (Figure 3A,B), in agreement with previous findings.[28,29] The Raman data show a modest red tail just below 3000 cm^{-1} for the O−H stretch mode in all three OH^- solutions (Figure 3A). This tail spans a significantly greater frequency range in the IR spectra (Figure 3B), reaching as low as ∼950 cm^{-1}. By contrast, KCl solutions have intensities that almost exactly match pure H_2O across this frequency range (Figure 3B). Therefore, the broad continuum found in hydroxide solutions can be attributed to the hydration sphere around OH^- anions.

An MCR algorithm (Figure 3C,D) was applied to these spectra to remove the background bulk water response. The resulting hydration shell spectra represent the minimum non-negative area difference between the hydroxide mixture spectra and pure water (see SI for more details).[30] When considering salt solutions, the MCR hydration shell spectra predominantly arise from anion hydration.[31−33] The dominance of anions

DOI: 10.1021/jacs.8b13458
J. Am. Chem. Soc. 2019, 141, 6930−6936

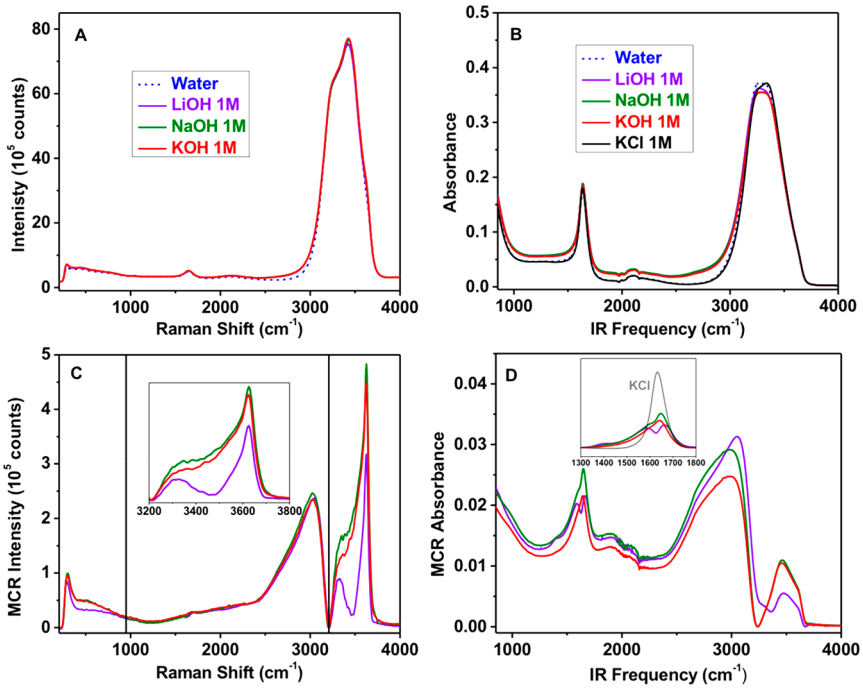

Figure 3. (A) Raman spectra of 1 M hydroxide solutions and neat water. (B) ATR-FTIR spectra of 1 M hydroxide solutions, neat water, and 1 M KCl. (C) Raman-MCR spectra of 1 M hydroxide solutions. The inset shows the frequency region corresponding to the localized proton O−H stretch vibrations. (D) IR-MCR spectra of 1 M hydroxide solutions. The inset shows the line shapes of the water bending mode as a function of counter cation for the hydroxide salts as well as for a 1 M KCl solution (gray).

over cations in these spectra should result from the different nature of water−cation and water−anion interactions. Namely, a small amount of electron density from the anions is donated into the antibonding orbitals of the surrounding hydration water molecules.[34,35] This leads to a significant perturbation of water vibrational modes. On the other hand, cations can only interact electrostatically with the oxygen atoms of their hydrating waters and thus have a smaller effect on the vibrational modes.[36]

The Raman-MCR spectra show a drop in intensity to near baseline around 3205 cm^{-1} for all three cations (Figure 3C). This frequency provides a remarkably clear demarcation line between the intensity for localized protons at higher frequencies and the more delocalized protons in the hydration shell of hydroxide between ∼950 and 3205 cm^{-1}. Anharmonic local-mode frequency analysis of AIMD snapshots supports these assignments (see SI Figure S4). By contrast with the Raman data, only the KOH and NaOH IR-MCR spectra display a similar minimum in this range, which is blue-shifted to near 3238 cm^{-1} (Figure 3D). The LiOH IR-MCR spectrum, however, has significant intensity around this frequency. Moreover, the LiOH IR-MCR data reveal greater proton delocalization in the hydroxide hydration shell as indicated by somewhat enhanced intensity below 3238 cm^{-1} as compared to Na^+ and K^+. This enhancement corresponds to protons in water O−H bonds that donate hydrogen bonds to OH^-, as will be described below. Nevertheless, the Raman-MCR spectrum for LiOH solutions displays essentially the same intensity as found for NaOH and KOH for the delocalized proton signature (intensity between the vertical black lines in Figure 3C), but substantially less intensity above 3205 cm^{-1}.

The reduced intensity in the high-frequency region of the LiOH Raman-MCR spectra compared to NaOH and KOH is related to the identity of the counterion and the concentration of solvent-shared ion pairs. The simplest interpretation of the Raman MCR data would be that contact ion pairs between Li^+ and OH^- lead to fewer first hydration shell water molecules around the hydroxide ion. However, the integrated ion pairing number densities from AIMD simulations speak against this idea (Figure 2) and show that there is only a minimal number of contact ion pairs in either LiOH or NaOH at 1 M concentration. Li^+ is well hydrated and small, which allows this cation to sit closer to and interact more strongly with a bridging water in solvent-shared ion pairs as revealed in AIMD simulations (Figure 2). In light of these results, quantum chemical calculations (MP2/aug-cc-pVTZ) for the Raman cross section of optimized H_2O−Li^+ and H_2O−Na^+ complexes in the gas phase were conducted and showed that Li^+ diminishes the water symmetric stretch Raman intensity by ∼50% relative to Na^+. The substantially higher concentration of more closely spaced solvent-shared ion pairs in LiOH, along with the greater attenuation of Raman intensities by Li^+ compared to Na^+, support the idea that the dip in the MCR-Raman spectra at ∼3470 cm^{-1} (inset of Figure 3C) is a result of solvent-shared ion pairing. Na^+ can also cause a dip at this frequency, when 6 M NaOH is in solution (Figure S5). Of course, in this case, the salt saturation limit has been reached and the fraction of Na^+ solvent-shared ion pairs is quite substantial.

Additional Raman-MCR data were taken with 0.5 M LiOH, and a similar intensity attenuation was found in the low- and high-frequency regions as for 1.0 M LiOH (Figure S6). This is strong evidence that ion pairing persists below 1 M in the case of this salt. These results stand in sharp contrast to data for acid solutions (e.g., HCl), where the lowest concentration at which ion pairing could be detected between acid protons and halide anions was just above 2 M.[20,22,39] Given these observations, it should be concluded that Li^+ interactions

DOI: 10.1021/jacs.8b13458
J. Am. Chem. Soc. 2019, 141, 6930−6936

with OH^- are significantly stronger than Cl^- interactions with H^+. Finally, the sharp feature at ~3630 cm^{-1} in the Raman-MCR spectra has long been assigned to the hydroxide ion stretch, and our calculations are consistent with this assignment (Figure S4).[18,28,29,37,38]

Potential Energy Curve Analysis. Consistent with previous studies, the AIMD simulations revealed a distinct hydration structure around the OH^- solute (Figure 4).[6,12]

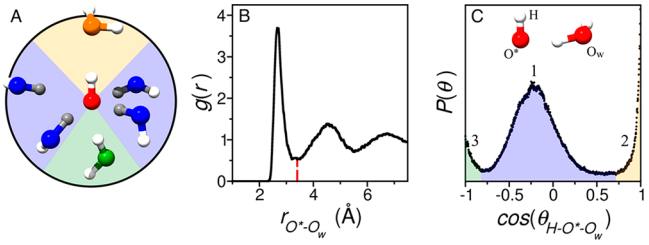

Figure 4. (A) Schematic representation of first solvation shell water molecules of hydroxide. Region 1 water molecules are shaded in blue. (B) The radial boundary of the first solvation shell is defined by the first minimum (vertical dashed red line) of the radial distribution function, $g(r)$, for the hydroxide oxygen, O*, to the water oxygen, O_W. (C) The angular boundaries of the three distinct regions of first solvation shell water molecules are defined by the minima in the distribution of $\cos(H-O^*-O_W)$. The color coding in (C) corresponds to coding used in (A).

Based on structural analysis, the hydration shell water molecules were sorted into three regions using both distance (Figure 4B) and angular (Figure 4C) criteria. The first and most populated region is composed of water molecules donating hydrogen bonds to the OH^- oxygen (Figure 4A, blue shading, Region 1). Region 2 consists of water accepting a hydrogen bond from the OH^- hydrogen (orange shading), and Region 3 falls directly below the OH^- oxygen (green shading). The O−H bonds in Region 1 could be further sorted into Regions 1a and 1b, corresponding to OH groups donating hydrogen bonds to OH^- and OH groups donating hydrogen bonds to second hydration shell water molecules, respectively.

Different degrees of proton delocalization in the AIMD simulations can be quantified through a delocalization parameter, σ, which is defined as the full width at half-maximum (FWHM) of the proton probability density ($|\Psi_0|^2$) in the vibrational ground state as shown in Figure 5. Region 1a protons are quantum mechanically delocalized to a greater extent than other protons in the hydration shell. For comparison, $\langle\sigma\rangle$ for Region 1a protons averaged over all snapshots was 0.382 and 0.376 Å for the LiOH and NaOH simulations, respectively. Averages for every other region in both simulations fell near the average of bulk water simulations at 0.336 Å (Table S4). Moreover, Region 1a protons gave rise to vibrational intensity primarily between 1000 and 3200 cm^{-1}, while localized protons (Regions 1b, 2, 3 in Figure 4) and the OH^- itself gave rise to intensity above 3200 cm^{-1} (Figure S4). These calculations support the assignments of distinct frequency regions in the vibrational spectra (Figure 3). Although there are typically three or four water molecules donating hydrogen bonds to the OH^- oxygen within the dynamical hypercoordination mechanism, the delocalization mapping shows that there is always one Region 1a proton that is more delocalized than the others (Figure 5C, yellow proton). This is consistent with the concept of a "most active" hydrogen bond within the confines of the dynamical hypercoordination mechanism.[6,10] Furthermore, Region 1a protons are shared more evenly between oxygen nuclei compared to Region 1b protons (i.e., the proton position in Figure 5A is closer to zero than in Figure 5B).

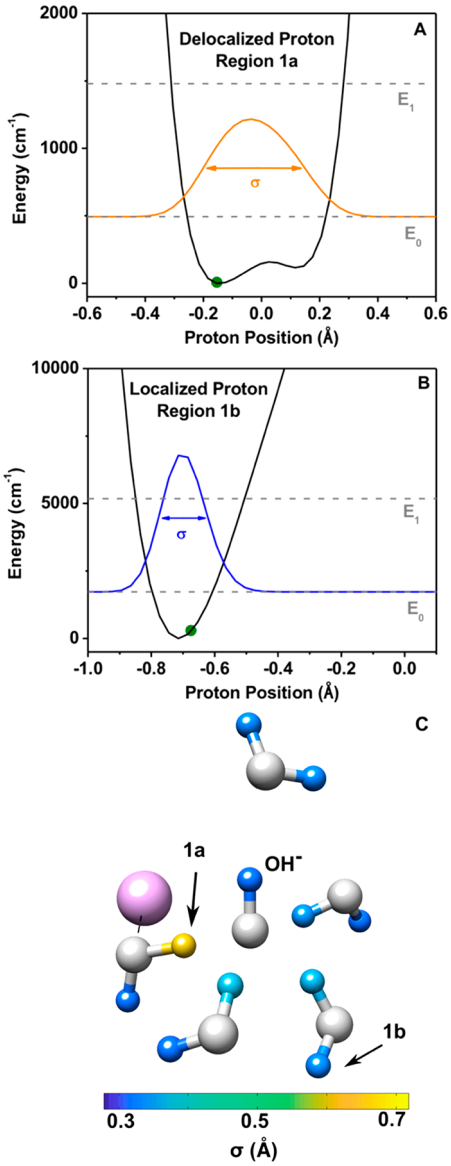

Figure 5. (A) Potential energy curve (shown in black) of a Region 1a proton. The ground and first excited state energy levels are depicted by gray, dashed lines, while the ground state proton wave function squared, $|\Psi_0|^2$, is represented by the orange curve. (B) Potential energy curve (shown in black) of a Region 1b proton, ground and first excited state energy levels (gray, dashed lines), and $|\Psi_0|^2$ (blue). Different scalings of x- and y-axes are used in (A) and (B). Negative x-axis positions correspond to protons closer to the hydration shell water oxygen, and positive positions correspond to the proton being closer to (A) the hydroxide oxygen and (B) a second hydration shell water oxygen, respectively. The green circles on each potential energy curve depict the classical position of each proton, respectively. (C) Delocalization heat map of a hydrated hydroxide complex from the 1.0 M LiOH simulation, where σ is calculated as depicted in (A) and (B). The data in (A) correspond to the yellow proton labeled 1a, and the same for the data in (B) and the blue 1b proton. Each of these protons are marked with an arrow. All oxygen atoms are colored gray to highlight differences in σ between the protons. The purple sphere represents Li^+.

DOI: 10.1021/jacs.8b13458
J. Am. Chem. Soc. 2019, 141, 6930−6936

Interpreting the Vibrational Spectra with AIMD. By contrast with the Raman spectra, the transition dipole moments in the IR spectra for the delocalized protons are far more sensitive to the local environment of the proton (Figure 3D).[38−41] As a result, IR-MCR hydration shell spectra can report on proton delocalization as a function of counter cation identity. These spectra display subtly enhanced intensity in the presence of Li^+ relative to Na^+ or K^+ counter cations at frequencies that can be assigned to Region 1a protons. As noted above, in the Li^+ spectrum, the IR-MCR intensity does not show a pronounced minimum near 3238 cm^{-1}. This suggests proton sharing is enhanced in LiOH solutions. This result raises an interesting question as to how counter cations influence proton sharing. As such, in the AIMD simulations, we focused on snapshots with a solvent-shared water molecule between OH^- and a metal cation. Specifically, the average displacement coordinate, $\langle\delta\rangle$, $\langle\sigma\rangle$, and the transition dipole moment integral (TDMI) were calculated for any Region 1a proton within a solvent-shared ion pair for the LiOH and NaOH trajectories (Table 1).

Table 1. Averages of the Proton Displacement Coordinate, $\langle\delta\rangle$, the fwhm of the Ground Vibrational State Proton Density, $\langle\sigma\rangle$, and the Transition Dipole Moment Integral, $\langle\psi_0|\mu|\psi_1\rangle$, for Solvent-Shared Ion Pairs[a]

solution	$\langle\delta\rangle$ (Å)	$\langle\sigma\rangle$ (Å)	$\langle\psi_0\|\mu\|\psi_1\rangle$ (D)
LiOH, 1 M	−0.868 (0.075)	0.383 (0.016)	112.3 (27.6)
NaOH, 1 M	−0.970 (0.072)	0.367 (0.019)	84.2 (32.8)

[a]Solvent-shared ion pairs occur when a water molecule simultaneously resided in the first hydration shell of both hydroxide and a counter cation. Standard deviations of the averages are included in parentheses.

Based on these calculations, the modest enhancement of Region 1a intensity in the IR-MCR spectra of LiOH arose from greater proton sharing within $Li^+{-}OH_2{-}OH^-$ complexes. The proton displacement coordinate is defined using the classical position of the proton nucleus (green dots in Figure 5A,B) as $\delta = R_{OaH} - R_{ObH}$, where O_a is the hydration shell water oxygen and O_b is the hydroxide oxygen.[5] Given this definition, the displacement coordinate values will always be negative. The closer in magnitude δ is to zero, the more equally shared a proton is between the oxygen nuclei of hydroxide and the first shell water. As shown in Table 1, Region 1a protons are shared more equally between the oxygen nuclei adjacent to Li^+ compared with Na^+. This trend is also observed in the average σ value. Namely, the average is slightly broader for Li^+, indicating that protons are more quantum mechanically delocalized than in the presence of Na^+. Moreover, the calculated TDMI values from Table 1 roughly correlate to the spectral intensity observed in the experimental IR-MCR spectra (Figure 3D).

Finally, the bending mode is split in the OH^- IR-MCR spectra in the presence of Li^+ (Figure 3D inset). The line shape is similar to that from direct subtraction difference spectra and MCR spectra for hydrated proton IR data.[17,39,42] These findings suggest that the splitting of the bending mode for the hydration shell water in 1D spectra reports on sharing of proton nuclei. To explore this point further, experiments were performed in D_2O and showed significantly less splitting (Figure S8). This was expected, as delocalization and sharing should be attenuated in deuterated samples.[6] Also, the inset in Figure 4D shows that switching from hydroxide solutions to KCl completely removed the splitting as well as the intensity on the low-frequency side of the bending resonance. Therefore, the splitting is indeed related to the presence of the hydroxide. In the hydroxide solutions, there is a strong dependence for the splitting on the counter cation. The greatest splitting is observed in LiOH solutions, followed by NaOH, and then KOH. Based on these results, there appears to be enhanced proton delocalization and sharing in solutions containing Li^+ relative to other cations.

Diffusion Data and Vibrational Spectra. The diffusion constant data in Figure 1 clearly show that mobility is lower in the presence of Li^+ compared to the other two cations. On the other hand, the IR-MCR data indicate more proton delocalization with Li^+ (Figure 3D). As such, there is not a straightforward relationship between the extent of proton delocalization in water molecules that are hydrogen bonded to hydroxide and the overall OH^- diffusion process. Li^+ counter cations have higher charge density than the other monovalent metal cations and polarize water around OH^- more efficiently. Moreover, water protons coordinating with the hydroxide oxygen are less tightly bound to the donating water molecule and more delocalized across the transfer coordinate with Li^+ compared to Na^+ or K^+. This increased delocalization, however, does not translate into increased solution conductivity and faster diffusion. In fact, despite the increased proton delocalization, Li^+ exhibits stronger electrostatic attraction and ion pairing to OH^-, which reduces the diffusion coefficient, rather than enhancing it. Such pairing explains the slower diffusion of ions in LiOH solutions at concentrations as low as 10 mM, where simple additivity fails to explain the experimental data.

CONCLUSIONS

Herein, we have shown that specific cation effects are important for hydroxide mobility and proton sharing in hydroxide solutions. AIMD simulations and experimental vibrational hydration shell spectra suggest strong electrostatic attraction between OH^- and Li^+ cations that results in stronger ion pairing than with other cations. This ion pairing is stronger than that previously reported in acidic solutions and persists into more dilute solutions. Li^+ enhances proton sharing in the first hydration shell compared with other cations, but this does not lead to an enhancement in the diffusion coefficient. In fact, direct interactions with well-hydrated counter cations impede OH^- mobility.

ASSOCIATED CONTENT

Supporting Information

The Supporting Information is available free of charge on the ACS Publications website at DOI: 10.1021/jacs.8b13458.

Experimental materials and procedures, computational methods, fits for EIS data, isotope effects on IR-MCR spectra, calculated spectral data, ion pairing analysis, and calculated spectra of 0.5 M OH^- simulation (PDF)

AUTHOR INFORMATION

Corresponding Authors

*Steven.A.Corcelli.1@nd.edu

*psc11@psu.edu

ORCID

Chad I. Drexler: 0000-0002-9989-968X

DOI: 10.1021/jacs.8b13458
J. Am. Chem. Soc. 2019, 141, 6930−6936

Yuguang C. Li: 0000-0002-9559-7051
Steven A. Corcelli: 0000-0001-6451-4447
Paul S. Cremer: 0000-0002-8524-0438

Author Contributions

#C.I.D. and T.C.M. contributed equally.

Notes

The authors declare no competing financial interest.

■ ACKNOWLEDGMENTS

P.S.C. thanks the National Science Foundation (CHE-1709735) for support. We thank Dor Ben-Amotz for providing the SMCR software in Igor Pro and for insightful discussions in implementing the algorithm. We thank Tawanda Zimudzi and Josh Stapleton of Penn State's Materials Characterization Lab for help with the collection of IR data. We thank Thomas E. Mallouk for insightful discussions concerning EIS data and equivalent electrochemical circuit models. S.A.C. thanks the National Science Foundation (CHE-1565471) for support. The authors are grateful for high-performance computing resources and support from the Center for Research Computing at the University of Notre Dame. This work used the Extreme Science and Engineering Discovery Environment (XSEDE), which is supported by National Science Foundation grant number ACI-1548562. XSEDE resources Bridges at Pittsburgh Supercomputing Center and Comet at San Diego Supercomputer Center were used through allocations TG-CHE180017, TG-TRA140029, and TG-PHY130048.

■ REFERENCES

(1) Duso, A. B.; Chen, D. D. Y. Proton and Hydroxide Ion Mobility in Capillary Electrophoresis. *Anal. Chem.* **2002**, *74* (13), 2938−2942.
(2) Johnston, J. The Change of the Equivalent Conductance of Ions with the Temperature. *J. Am. Chem. Soc.* **1909**, *31* (9), 1010−1020.
(3) Noyes, A. A.; Kato, Y. The Equivalent Conductance of Hydrogen-Ion Derived from Transference Experiments with Nitric Acid. *J. Am. Chem. Soc.* **1908**, *30* (3), 318−334.
(4) Robinson, R. A.; Stokes, R. H. *Electrolyte Solutions*, 2nd ed.; Butterworths: London, 1959.
(5) Marx, D. Proton Transfer 200 Years after von Grotthuss: Insights from *Ab Initio* Simulations. *ChemPhysChem* **2006**, *7* (9), 1848−1870.
(6) Marx, D.; Chandra, A.; Tuckerman, M. E. Aqueous Basic Solutions: Hydroxide Solvation, Structural Diffusion, and Comparison to the Hydrated Proton. *Chem. Rev.* **2010**, *110* (4), 2174−2216.
(7) Onsager, L. The Motion of Ions: Principles and Concepts. *Science* **1969**, *166* (3911), 1359−1364.
(8) Agmon, N.; Bakker, H. J.; Campen, R. K.; Henchman, R. H.; Pohl, P.; Roke, S.; Thämer, M.; Hassanali, A. Protons and Hydroxide Ions in Aqueous Systems. *Chem. Rev.* **2016**, *116* (13), 7642−7672.
(9) Marx, D.; Tuckerman, M. E.; Hutter, J.; Parrinello, M. The Nature of the Hydrated Excess Proton in Water. *Nature* **1999**, *397* (6720), 601−604.
(10) Tuckerman, M. E.; Marx, D.; Parrinello, M. The Nature and Transport Mechanism of Hydrated Hydroxide Ions in Aqueous Solution. *Nature* **2002**, *417* (6892), 925−929.
(11) Hassanali, A.; Giberti, F.; Cuny, J.; Kühne, T. D.; Parrinello, M. Proton Transfer through the Water Gossamer. *Proc. Natl. Acad. Sci. U. S. A.* **2013**, *110* (34), 13723−13728.
(12) Chen, M.; Zheng, L.; Santra, B.; Ko, H.-Y.; Jr, R. A. D.; Klein, M. L.; Car, R.; Wu, X. Hydroxide Diffuses Slower than Hydronium in Water Because Its Solvated Structure Inhibits Correlated Proton Transfer. *Nat. Chem.* **2018**, *10* (4), 413.
(13) Walrafen, G. E.; Yang, W.-H.; Chu, Y. C. High-Temperature Raman Investigation of Concentrated Sulfuric Acid Mixtures: Measurement of H-Bond Values between H_3O^+ or $H_5O_2^+$ and HSO_4^-. *J. Phys. Chem. A* **2002**, *106* (43), 10162−10173.
(14) Janoschek, R.; Weidemann, E.; Zundel, G. Calculated Frequencies and Intensities Associated with Coupling of the Proton Motion with the Hydrogen Bond Stretching Vibration in a Double Minimum Potential Surface. *J. Chem. Soc., Faraday Trans. 2* **1973**, *69* (0), 505−520.
(15) Roberts, S. T.; Petersen, P. B.; Ramasesha, K.; Tokmakoff, A.; Ufimtsev, I. S.; Martinez, T. J. Observation of a Zundel-like Transition State during Proton Transfer in Aqueous Hydroxide Solutions. *Proc. Natl. Acad. Sci. U. S. A.* **2009**, *106* (36), 15154−15159.
(16) Mandal, A.; Ramasesha, K.; De Marco, L.; Tokmakoff, A. Collective Vibrations of Water-Solvated Hydroxide Ions Investigated with Broadband 2DIR Spectroscopy. *J. Chem. Phys.* **2014**, *140* (20), 204508.
(17) Thämer, M.; Marco, L. D.; Ramasesha, K.; Mandal, A.; Tokmakoff, A. Ultrafast 2D IR Spectroscopy of the Excess Proton in Liquid Water. *Science* **2015**, *350* (6256), 78−82.
(18) Walrafen, G. E.; Douglas, R. T. W. Raman Spectra from Very Concentrated Aqueous NaOH and from Wet and Dry, Solid, and Anhydrous Molten, LiOH, NaOH, and KOH. *J. Chem. Phys.* **2006**, *124* (11), 114504.
(19) Mandal, A.; Tokmakoff, A. Vibrational Dynamics of Aqueous Hydroxide Solutions Probed Using Broadband 2DIR Spectroscopy. *J. Chem. Phys.* **2015**, *143* (19), 194501.
(20) Baer, M. D.; Fulton, J. L.; Balasubramanian, M.; Schenter, G. K.; Mundy, C. J. Persistent Ion Pairing in Aqueous Hydrochloric Acid. *J. Phys. Chem. B* **2014**, *118* (26), 7211−7220.
(21) Walewski, Ł.; Forbert, H.; Marx, D. Quantum Induced Bond Centering in Microsolvated HCl: Solvent Separated versus Contact Ion Pairs. *J. Phys. Chem. Lett.* **2011**, *2* (24), 3069−3074.
(22) Fulton, J. L.; Balasubramanian, M. Structure of Hydronium (H_3O^+)/Chloride (Cl^-) Contact Ion Pairs in Aqueous Hydrochloric Acid Solution: A Zundel-like Local Configuration. *J. Am. Chem. Soc.* **2010**, *132* (36), 12597−12604.
(23) Gutberlet, A.; Schwaab, G.; Birer, Ö.; Masia, M.; Kaczmarek, A.; Forbert, H.; Havenith, M.; Marx, D. Aggregation-Induced Dissociation of $HCl(H_2O)_4$ Below 1 K: The Smallest Droplet of Acid. *Science* **2009**, *324* (5934), 1545−1548.
(24) Tuckerman, M. E.; Chandra, A.; Marx, D. Structure and Dynamics of OH^-(aq). *Acc. Chem. Res.* **2006**, *39* (2), 151−158.
(25) Zhu, Z.; Tuckerman, M. E. Ab Initio Molecular Dynamics Investigation of the Concentration Dependence of Charged Defect Transport in Basic Solutions via Calculation of the Infrared Spectrum. *J. Phys. Chem. B* **2002**, *106* (33), 8009−8018.
(26) Marcus, Y.; Hefter, G. Ion Pairing. *Chem. Rev.* **2006**, *106* (11), 4585−4621.
(27) Noulty, R. A.; Leaist, D. G. Activity Coefficients and Diffusion Coefficients of Dilute Aqueous Solutions of Lithium, Sodium, and Potassium Hydroxides. *J. Solution Chem.* **1984**, *13* (11), 767−778.
(28) Corridoni, T.; Sodo, A.; Bruni, F.; Ricci, M. A.; Nardone, M. Probing Water Dynamics with OH^-. *Chem. Phys.* **2007**, *336* (2), 183−187.
(29) Sbroscia, M.; Sodo, A.; Bruni, F.; Corridoni, T.; Ricci, M. A. OH Stretching Dynamics in Hydroxide Aqueous Solutions. *J. Phys. Chem. B* **2018**, *122* (14), 4077−4082.
(30) Fega, K. R.; Wilcox, A. S.; Ben-Amotz, D. Application of Raman Multivariate Curve Resolution to Solvation-Shell Spectroscopy. *Appl. Spectrosc.* **2012**, *66* (3), 282−288.
(31) Perera, P. N.; Browder, B.; Ben-Amotz, D. Perturbations of Water by Alkali Halide Ions Measured Using Multivariate Raman Curve Resolution. *J. Phys. Chem. B* **2009**, *113* (7), 1805−1809.
(32) Yoshimura, Y.; Kanno, H. Cationic Effects in the Raman OD Stretching Spectra of Aqueous Electrolyte Solutions. *J. Raman Spectrosc.* **1996**, *27* (9), 671−674.
(33) Walrafen, G. E. Raman Spectral Studies of the Effects of Perchlorate Ion on Water Structure. *J. Chem. Phys.* **1970**, *52* (8), 4176−4198.

DOI: 10.1021/jacs.8b13458
J. Am. Chem. Soc. 2019, 141, 6930−6936

(34) Lee, H.; Choi, J.-H.; Cho, M. Vibrational Solvatochromism and Electrochromism of Cyanide, Thiocyanate, and Azide Anions in Water. *Phys. Chem. Chem. Phys.* **2010**, *12* (39), 12658−12669.
(35) Bajaj, P.; Götz, A. W.; Paesani, F. Toward Chemical Accuracy in the Description of Ion-Water Interactions through Many-Body Representations. I. Halide-Water Dimer Potential Energy Surfaces. *J. Chem. Theory Comput.* **2016**, *12* (6), 2698−2705.
(36) Galib, M.; Baer, M. D.; Skinner, L. B.; Mundy, C. J.; Huthwelker, T.; Schenter, G. K.; Benmore, C. J.; Govind, N.; Fulton, J. L. Revisiting the Hydration Structure of Aqueous Na^+. *J. Chem. Phys.* **2017**, *146* (8), 84504.
(37) Hermansson, K.; Bopp, P. A.; Spångberg, D.; Pejov, L.; Bakó, I.; Mitev, P. D. The Vibrating Hydroxide Ion in Water. *Chem. Phys. Lett.* **2011**, *514* (1−3), 1−15.
(38) Mondal, J. A.; Namboodiri, V.; Mathi, P.; Singh, A. K. Alkyl Chain Length Dependent Structural and Orientational Transformations of Water at Alcohol-Water Interfaces and Its Relevance to Atmospheric Aerosols. *J. Phys. Chem. Lett.* **2017**, *8* (7), 1637−1644.
(39) Daly, C. A.; Streacker, L. M.; Sun, Y.; Pattenaude, S. R.; Hassanali, A. A.; Petersen, P. B.; Corcelli, S. A.; Ben-Amotz, D. Decomposition of the Experimental Raman and Infrared Spectra of Acidic Water into Proton, Special Pair, and Counterion Contributions. *J. Phys. Chem. Lett.* **2017**, *8* (21), 5246−5252.
(40) Schmidt, J. R.; Corcelli, S. A.; Skinner, J. L. Pronounced Non-Condon Effects in the Ultrafast Infrared Spectroscopy of Water. *J. Chem. Phys.* **2005**, *123* (4), 44513.
(41) Auer, B.; Kumar, R.; Schmidt, J. R.; Skinner, J. L. Hydrogen Bonding and Raman, IR, and 2D-IR Spectroscopy of Dilute HOD in Liquid D_2O. *Proc. Natl. Acad. Sci. U. S. A.* **2007**, *104* (36), 14215−14220.
(42) Fournier, J. A.; Carpenter, W. B.; Lewis, N. H. C.; Tokmakoff, A. Broadband 2D IR Spectroscopy Reveals Dominant Asymmetric $H_5O_2^+$ Proton Hydration Structures in Acid Solutions. *Nat. Chem.* **2018**, *10* (9), 932.

DOI: 10.1021/jacs.8b13458
J. Am. Chem. Soc. 2019, 141, 6930−6936